



Facile synthesis of nano dendrite-structured Ni–NiO foam/ERGO by constant current method for supercapacitor applications

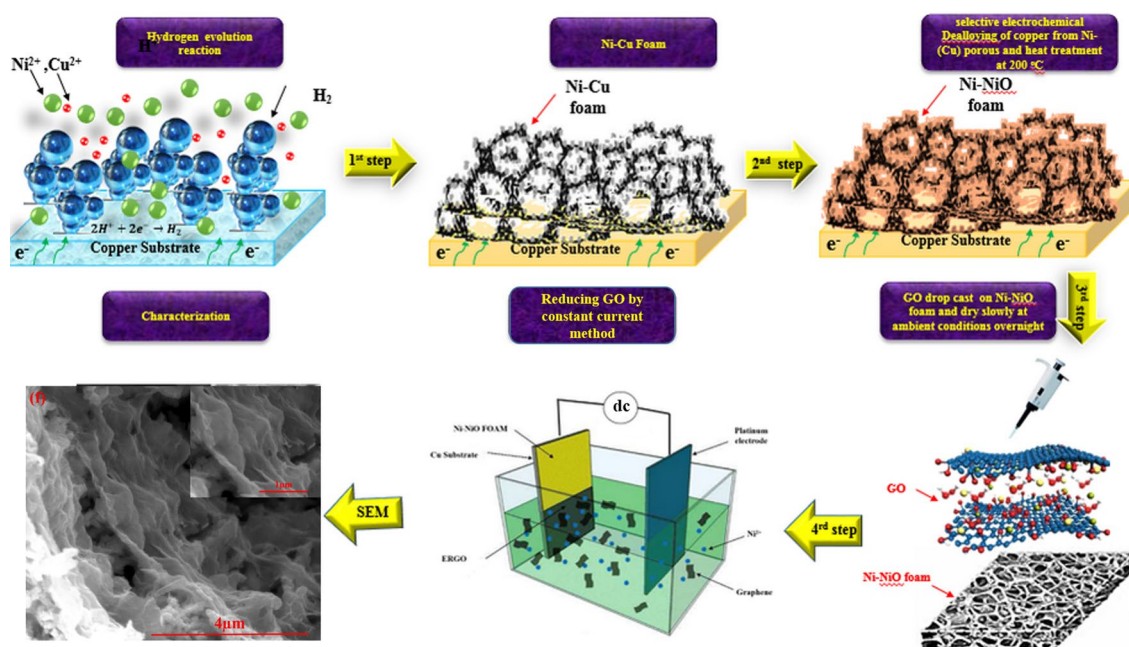
Majid Mirzaee¹ · Changiz Dehghanian¹ · Sahand Sarbishei²

Received: 13 March 2018 / Accepted: 7 June 2018 / Published online: 23 June 2018
© Springer Nature B.V. 2018

Abstract

This study introduces a novel, non-toxic, scalable, two-step method for the fabrication of highly nanoporous nickel and nickel oxide (Ni–NiO) foam/Electrochemically reduced graphene oxide (ERGO) electrodes with exceptional capacitance suitable for supercapacitor application. This procedure includes drop cast and graphene oxide (GO) reduction by galvanostatic process. To create the electrodes, electrodeposition process and selective electrochemical dealloying accompanied by a hydrogen evolution reaction (HER) were performed on a copper substrate. Afterwards, drop cast and galvanostatic processes were accomplished to coat GO nanosheets on Ni–NiO foam. The structure of achieved nanocomposites was investigated by scanning electron microscopy (SEM), X-ray diffraction (XRD), Raman spectroscopy, and X-ray photoelectron spectroscopy (XPS). High-specific capacitance of 1995 F g^{-1} at a current density of 1 A g^{-1} (galvanostatic charge–discharge) (GCD) was achieved for the Ni–NiO foam/electrochemically reduced graphene oxide (ERGO) electrode with excellent cycling stability. A constant, high-specific capacitance (95.1% of the initial value) was achieved after 6000 cycles at 20 A g^{-1} .

Graphical Abstract



Keywords ERGO · Ni–NiO foam · Supercapacitor · Electrochemical reduction · Constant current

1 Introduction

Electrochemical supercapacitors, also known as ultracapacitors due to their high capacitance, power density, and life-cycle stability and fast recharging capability, have been considered as the next generation of energy storage devices [1]. The supercapacitors include electrical double-layer capacitors (EDLCs) and pseudocapacitors. Various kinds of materials such as transition-metal oxides and conducting polymers have been considered for pseudocapacitor application [2]. Scholars have done several research studies to raise the surface area of electroactive materials to induce high-specific capacitance. In this regard, an easy fabrication process such as electrochemical deposition accompanied with a hydrogen evolution reaction has been developed [3, 4]. Hydrogen evolution results in the formation of a high surface area electrode of dendritic structure with numerous pores [5–7]. The use of high conductivity materials such as graphite, carbon nanotube, and graphene in the electrodes can increase the electrical conductivity of metal oxide electrodes [8–11]. In this regard, graphene is a suitable matrix for the growth of metal oxides due to its high conductivity, electrochemical stability, great surface area, and superior mechanical properties. Combining graphene as the active metal oxide with the nanocomposite can increase electrical conductivity and mechanical strength of product. Moreover, the supply of 3D porous architectures by skeletons with the interconnected pores results in the higher surface area of active materials and easier ion diffusion [12–15]. Although NiO is known as electrode material, its low electrical conductivity leads to high internal resistance and poor performance in electrochemical devices [16, 17]. In this work, a dendritic Ni–NiO foam was created by electrodeposition in a hydrogen evolution reaction. Numerous dendritic morphologies with high surface area were fabricated by the application of high cathodic overpotential to a conductive substrate. Furthermore, the selective electrochemical dealloying of copper from Ni–Cu alloy was employed to create nanoporous dendritic Ni–NiO foam. For this purpose, the GO films were prepared by the drop casting of a dilute GO dispersion on Ni–NiO foam electrodes and then dried in ambient conditions. Next, as-prepared GO films on the Ni–NiO foam electrodes were electrochemically reduced in the current density ranging from -0.6 to -20 mA cm $^{-2}$ in a 1 M KOH electrolyte. The combination of redox reaction of elemental nickel and GO in the preparation stages of Ni–NiO foam/ERGO composites facilitated the preparation process and improved the adhesion and contact between the Ni–NiO foam and ERGO. Raman spectroscopy, XRD, and XPS were used to investigate structural changes in electrodes. Furthermore,

supercapacitor characteristics of the samples fabricated at different reduction current densities were studied by cyclic voltammetry (CV), electrochemical impedance spectroscopy (EIS), and GCD. The generated Ni–NiO electrodes showed an excellent electrochemical capacitance and good stability for supercapacitors.

2 Experiments

2.1 Chemicals and synthesis of Ni–NiO foam

The porous structure of Ni–NiO foam can be prepared by electrodeposition method by means of HER [18]. In this study, however, copper as co-alloyed material was employed in a simple electrochemical dealloying method in sulfuric acid to obtain dendritic and porous Ni–NiO. Three-electrode cell was utilized to fabricate dendritic Ni–NiO foam electrode. In this regard, copper plate (1×1 cm 2), saturated calomel electrode (SCE), and platinum electrode (1×4 cm 2) were applied as working, reference, and counter electrodes, respectively. Electrodeposition process was carried out at a constant current density of 2 A cm $^{-2}$ using a Solartron 1278 potentiostat for a deposition time of 180 s in an electrolyte containing 0.5 M NiSO $_4 \cdot 7$ H $_2$ O, 1.5 M H $_2$ SO $_4$, 1 M HCl, and 0.01 M CuSO $_4 \cdot 5$ H $_2$ O. Subsequently, nanoporous Ni–NiO electrode was fabricated by the electrochemical dealloying of copper at 0.5 V in a 1 M H $_2$ SO $_4$ solution on dendritic Ni–Cu alloy foam. The heat treatment of selected samples was performed in a Memmert oven at 200 °C for 1 h.

2.2 Preparation of GO dispersion

The hammer method and exfoliation by sonication were employed to synthesize GO from graphite flakes (GF) [19].

2.3 Preparation of GO and ERGO films for electrochemical characterization

1 mg ml $^{-1}$ GO dispersion was fabricated by the ultrasonic exfoliation of graphite oxide powder in a 0.067 M phosphate buffer solution (PBS) with a pH of 9.18. ERGO electrodes were prepared by the drop casting of 20 μ l GO dispersion (1 mg ml $^{-1}$) on the Ni–NiO foam electrodes. Afterwards, electrodes were left overnight to dry in ambient conditions. The reduction process of each ERGO electrode was conducted at a constant current density ranging from -0.6 to -20 mA cm $^{-2}$ for a duration of 200 s in a standard three-electrode electrochemical cell containing 1 M KOH electrolyte.

2.4 Structural characterization

Raman spectra were analyzed by means of a Horiba Jobin Yvon LabRAM in a 100-objective lens and a 632 nm laser. The XPS were obtained by thermo electron multilab 2000. Before the XPS measurement, all samples were dried in vacuum. The XPS narrow scan photo peak spectrum of the C1s region was carried out, and the peak-fit analyses were performed by the casa XPS software. Moreover, SEM (CamScan- MV2300) and XRD, Philips PC-APD with Cu K α radiation were used to investigate the morphology and phase composition (OR morphology, chemical composition, and crystallographic characteristics) of the deposited foams. Fourier-transform infrared (FT-IR) spectroscopy was performed by the use of a Bruker Tensor 27 spectrometer in the range from 400 to 4000 cm⁻¹.

2.5 Electrochemical characterization

The electrochemical measurements were done by a Solartron 1278 potentiostat using three-electrode cell containing a 1 M KOH aqueous solution. CV was carried out between -0.1 and 0.5 V at 25 °C using the 3D porous Ni–NiO foam/ERGO composite film, SCE, and a Pt foil as the working, reference, and counter electrodes, respectively. EIS measurements were performed with a superimposed 5 mV sinusoidal voltage in the frequency range of 10⁵–10⁻² Hz. The GCD tests were conducted by a Solartron 1278 potentiostat with a constant current density of 20 A g⁻¹ for 6000 cycles. The average specific capacitance values were obtained from CV curves according to the subsequent equation:

$$C = \frac{\int IdV}{vm\Delta V}, \quad (1)$$

where I , m , v , and ΔV are the voltammetric current, mass of the whole solid electrode material, potential scan rate, and potential in one sweep subdivision, respectively. The specific capacitance was also calculated from galvanostatic discharge using the following equation:

$$C = \frac{I\Delta t}{m\Delta V} \quad (2)$$

in which I denotes the discharge current, Δt and m are the time for a complete discharge and mass of the total solid electrode material, respectively, and ΔV represents the potential change after a complete discharge. The energy density (E) resulting from CV curves is calculated by Eq. (3)

$$E = \frac{1}{2}C(\Delta V)^2, \quad (3)$$

where C and ΔV are the average specific capacitance and potential extent of one sweep fragment. Power density (P) is obtained by the following equation:

$$P = \frac{E}{\Delta t}, \quad (4)$$

where E and Δt represent the energy density and period for one sweep fragment.

3 Results and discussion

3.1 Characterization by SEM

According to the SEM images of Ni–NiO foam electrode (Fig. 1a, b), numerous dendritic morphologies between 25 and 250 nm are observed. Due to the fact that metal atoms could not be deposited in the zone of hydrogen bubbles, the growth of ramified walls is influenced by two factors: arisen hydrogen bubbles from the platinum substrate and deposited metal by cathodic overpotential. Moreover, dendritic morphology is formed by intense hydrogen bubbles due to the instability of surface on the near electrode layer and change of hydrodynamic conditions [20]. In this regard, the size of dendritic morphology depends on the concentration of metal and H⁺ ions in the electrolyte. Furthermore, chlorine ions have considerable effects on hydrogen evolution and galvanic displacement reaction. For example, the displacement reaction of hydrogen evolution is powerfully delayed when chlorine ions are not available in sulfuric acid electrolyte. However, the addition of Cl⁻ ions into the sulfate-based electrolyte hastens the galvanic displacement reaction, and, as a result, hydrogen evolves dramatically, which leads to the formation of a dendritic structure [19]. According to the cross section image (Fig. 1c) and results of elemental map analysis, the wall thickness was made of numerous intertwined, packed nanodendrites. The thickness of the Ni–NiO foam processed for 180 s was 34.28 μm .

Figure 2a–g illustrates the surface morphology of the ERGO film prepared by a constant current density. The highly porous Ni–NiO foam was fabricated by drop casting combined with reduction process using constant current. Afterwards, Ni–NiO foam was covered by graphene sheet film, and the surface morphology of the Ni–NiO was modified. As observed, there is ragged surface morphology on the surface of the film, which is due to wrinkles of the graphene sheet film. Such morphology has advantages in the improvement of electron conductivity and increase of surface area between the electrolyte and electrode materials. Furthermore, the gap between the neighboring dendrites causes the easy diffusion of electrolyte, making dendrites in complete contact with electrolyte. Additionally, the uniform distribution of the ERGO sheets on the surface of the Ni–NiO foam can expose a higher area for electrochemical reactions. Such mesoporous structures are favorable for fast redox reactions and double-layer charging–discharging because of high mass

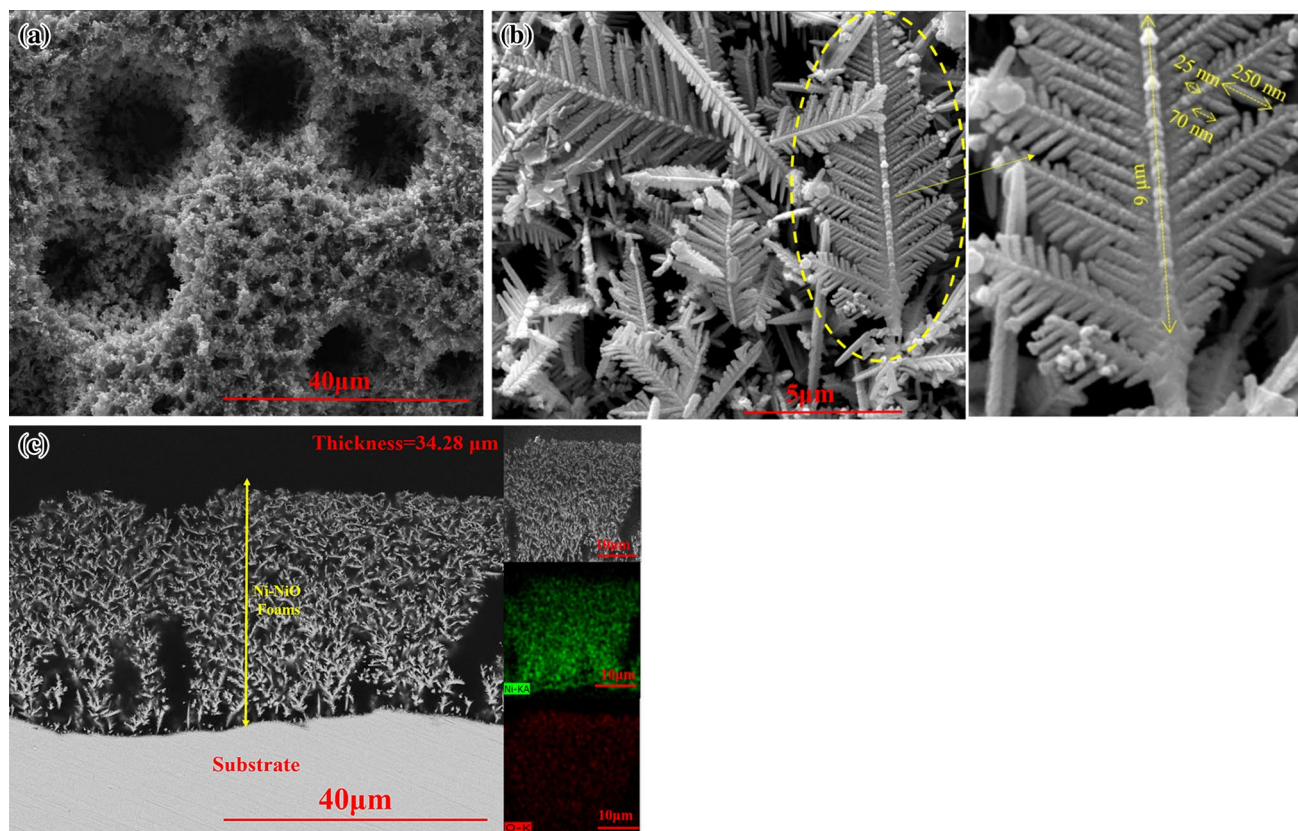


Fig. 1 a, b SEM views, c cross section of 3D Ni–NiO foams and map electrodeposited at 2 A cm^{-2} for 180 s on copper substrate

transportation between electrolyte and electrodes. Moreover, this type of structure can increase the electrode/electrolyte contact area greatly, resulting in enhanced electrochemical performance [20–22]. It should be mentioned that severe oxygen gas exhaustion was observed on the electrode in the current densities above -10 mA cm^{-2} , leading to the destruction of the coating.

3.2 Characterization by Raman spectroscopy

Figure 3 represents the Raman spectra of Ni–NiO foam/ERGO and Ni–NiO foam/GO, produced with the different reduction current densities. The peak at about 1327 cm^{-1} (D band) is associated with the defect and disorders in the graphitic layers, whereas the peak at about 1587 cm^{-1} (G band), corresponding to an E_{2g} mode of graphite, is related to the vibration of sp^2 -bonded carbon atoms in a two-dimensional, hexagonal lattice. It is generally accepted that the intensity ratio of the D–G bands (I_D/I_G) is a parameter reflecting the defect density of carbonaceous materials [23, 24]. The Raman spectra of GO, ERGO with reduction currents of -1.2 , -3.0 , -5.0 , and -10 mA cm^{-2} composites for D–G peak intensity ratios (I_D/I_G) of 0.89, 0.93, 0.95, 1.0, and 1.1, respectively, are shown in Fig. 3. It was found out that the electrochemical reduction

process removed most of the oxygen functional groups that were intercalated into the interlayer spacing of graphite. The electrochemical reduction of the exfoliated GO resulted in the depletion of the average size of the sp^2 domains due to the creation of abundant new graphitic domains that are smaller in size than the ones presented in the exfoliated GO during the process in the presence of the Ni and NiO foam [25, 26]. Moreover, two characteristic Raman peaks at around 515 and 1126 cm^{-1} are attributed to NiO [27–29]. According to Fig. 3, D and G bands of graphene in the Ni–NiO foam–graphene hybrid film were shifted to left with the increase in the current density. The band shift in carbon-based composites usually is associated with the charge transfer between carbon and other compounds [30, 31]. Therefore, the shift of Raman bands in the presence of NiO is attributed to the electrical interaction between NiO and the graphene sheet scaffold, leading to charge transport between the active material and substrate.

The size of the ERGO sheet synthesized in a reduction current of -10 mA cm^{-2} is calculated using Eq. (5) [32, 33]:

$$L_a(\text{nm}) = 2.4 \times 10^{-10} \times \lambda^4 \times \left(\frac{I_D}{I_G} \right)^{-1} \quad (5)$$

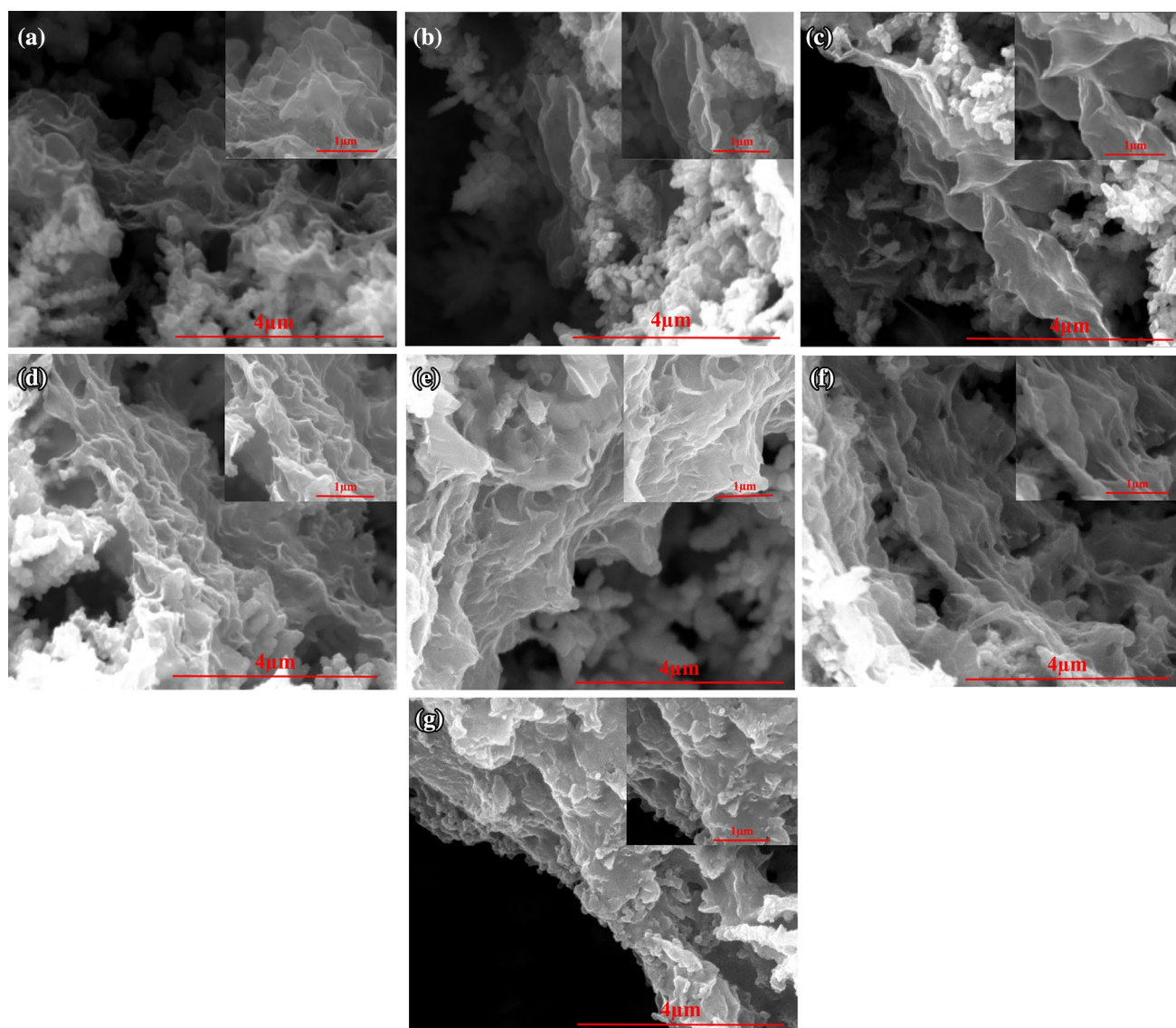


Fig. 2 The SEM images of the Ni–NiO foam/ERGO samples fabricated via a constant current method at current densities of **a** –0.6, **b** –1.2, **c** –1.8, **d** –3.0, **e** –5.0, **f** –10.0, and **g** –20.0 mA cm⁻²

In which λ is the stimulation wavelength. The graphene sheet size was calculated to be 34.12 nm

3.3 Characterization by X-ray photoelectron spectra

The chemical composition of the Ni–NiO foam/ERGO composite fabricated at a reduction current of -10 mA cm⁻² was examined by XPS. The results are presented in Fig. 4a–e. The XPS survey depicted in Fig. 4b represents carbon (C 1s), oxygen (O 1s), and Ni (Ni 2p), implying to the presence of these elements in the Ni–NiO foam/ERGO composite samples. The intensity of the C1s peak of GO is clearly much lower than that of the O1s peak (Fig. 4a), whereas the intensity of the C1s peak of ERGO is significantly higher

than that of the O1s (Fig. 4b). It confirms that most of the oxygen functional groups were depleted in the electrochemical reduction of the graphene sheet film. The high resolution of the C1s XPS spectra of GO and the Ni–NiO foam/ERGO composite is shown in Fig. 4c, d, indicating four different functional groups corresponding to non-oxygenated ring carbon (284.7 eV), carbon in C–O bonds (286.6 eV), carbonyl (287.9 eV), and carboxylate (289.1 eV). The previous peaks were also detected in the deconvolution of the C1s spectrum of ERGO. The comparison of the XPS spectra of the GO sheets and Ni–NiO foam/ERGO composite revealed a considerable decrease in the intensities of all C1s peaks of the oxygen containing functional groups, particularly, C (epoxy)/C–OH peak after the electrochemical reduction

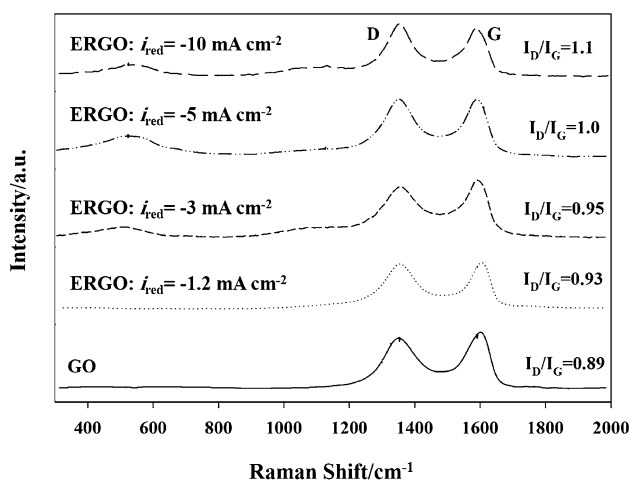


Fig. 3 The Raman spectra of GO and ERGO under the different constant reduction currents

process at -10 mA cm^{-2} . This result denotes that these oxygen functional groups were noticeably removed [34, 35]. Moreover, as shown in Fig. 4e, two main peaks at 872.8 and 855.2 eV in the Ni 2p XPS spectra are assigned to Ni $2p_{1/2}$ and Ni $2p_{3/2}$, respectively.

3.4 Characterization by XRD

The XRD patterns of the Ni–NiO foam–graphene hybrid film and Ni–NiO foam film, shown in Fig. 5, reveal that both samples were predominantly composed of the Ni foam. Moreover, the diffraction peaks observed for both films can be indexed as the (111), (200), and (220) for cubic NiO phase (JCPDS 4-0835) and Ni. A small diffraction peak was also detected at about $2\theta = 26.5^\circ$ in the NiO–graphene hybrid film, which is related to a (002) crystal plane of graphene (JCPDS 75-1621). The weight of Ni–NiO foam was measured by calculating the weight difference between the 3D porous Ni–NiO foam deposited on copper after electrodeposition and the copper. The load weight of Ni–NiO foam on copper substrate was approximately 6.36 mg cm^{-2} . Further, the percentage of Ni and NiO phase in foam was determined through X-ray intensity calculations using Eqs. (6) and (7).

$$\text{Percentage of NiO} = \frac{I_{\text{NiO}}}{I_{\text{NiO}} + I_{\text{Ni}}} \times 100 \quad (6)$$

$$\text{Percentage of Ni} = \frac{I_{\text{Ni}}}{I_{\text{Ni}} + I_{\text{NiO}}} \times 100 \quad (7)$$

I_{Ni} and I_{NiO} are the maximum X-ray intensity peaks of Ni and NiO in the patterns, respectively. The calculated Ni and NiO phases are 4.57 and 1.78 mg, respectively. The weight of ERGO was measured by calculating the weight difference

between the 3D porous Ni–NiO foam and the ERGO product after electrodeposition. The load weight of ERGO in the composite film for current density of -0.6 , -1.2 , -1.8 , -3.0 , -5.0 , and -10.0 were approximately 1.0, 1.03, 1.05, 1.09, 1.13, and 1.18 mg cm^{-2} , respectively.

3.5 Characterization by FT-IR

The Fourier-transform IR (FT-IR) was used to study the surface chemical structure of Ni–NiO foam/ERGO, Ni–NiO, and GO. As shown in Fig. 6, the $-\text{OH}$ (3376 cm^{-1}), $\text{C}=\text{O}$ (1732 cm^{-1}), and $\text{C}=\text{C}$ (1624 cm^{-1}) functional groups in GO were detected [36]. However, the typical peaks of $-\text{OH}$ (3376 cm^{-1}) and $\text{C}=\text{O}$ (1732 cm^{-1}) almost disappeared in Ni–NiO/ERGO due to the conversion of GO into ERGO. Normally, a $-\text{OH}$ peak at 3470 cm^{-1} is not detected for the Ni–NiO and Ni–NiO foam/ERGO samples after the thermal treatment at 200°C , but it was observed here owing to the water absorption of calcined micropores and nanodendrites during mixing and pelleting with KBr.

3.6 Supercapacitor electrochemical characterization

The reduction behavior of chronopotentiometry (CP) of GO on the Ni–NiO foam is depicted in Fig. 7. An increase in the current density caused the reduction potential to be raised, exhibiting the deposition of the conducting graphene on the Ni–NiO foam. Moreover, in current densities above -10 mA cm^{-2} , severe oxygen gas evolution was observed in the electrode, which reduces the adhesion of the coating and degrades it.

The performance of the composite electrode was further studied by EIS. Figure 8 presents the Nyquist plots of the Ni–NiO foam and Ni–NiO foam/ERGO reduced at -1.8 , -3 , -5 , -10 , and -20 mA cm^{-2} . These plots can be divided into the two regions: semicircle shape in the high frequency range, which is related to electron transfer limited process, and a straight line in the low frequency region, attributed to diffusion-limited electron transfer process [37, 38]. Equivalent series resistance (ESR) (R_s) and charge transfer resistance (R_{ct}) correspond to the x-interception of the plot at high frequency and diameter of the semicircle, respectively [44]. The ESR values, as shown in Fig. 8 (using ZSimpWin software), are 5.8Ω for $i = -1.8 \text{ mA cm}^{-2}$, 4.6Ω for $i = -3.0 \text{ mA cm}^{-2}$, 2.5Ω for $i = -5.0 \text{ mA cm}^{-2}$, 1.7Ω for $i = -10.0 \text{ mA cm}^{-2}$, 2.3Ω for $i = -20.0 \text{ mA cm}^{-2}$, and 11.3Ω for Ni–Ni foam. Obviously, the ERGO/Ni–NiO foam fabricated at $i = -10.0 \text{ mA cm}^{-2}$ provided the smallest ESR value, and thus the fastest charge/discharge process. The R_{ct} values obtained for ERGO/Ni–NiO foam composite electrodes are as follows: 1.8Ω ($i = -1.8 \text{ mA cm}^{-2}$), 1.3Ω ($i = -3.0 \text{ mA cm}^{-2}$), 0.9Ω ($i = -5.0 \text{ mA cm}^{-2}$), 0.6Ω

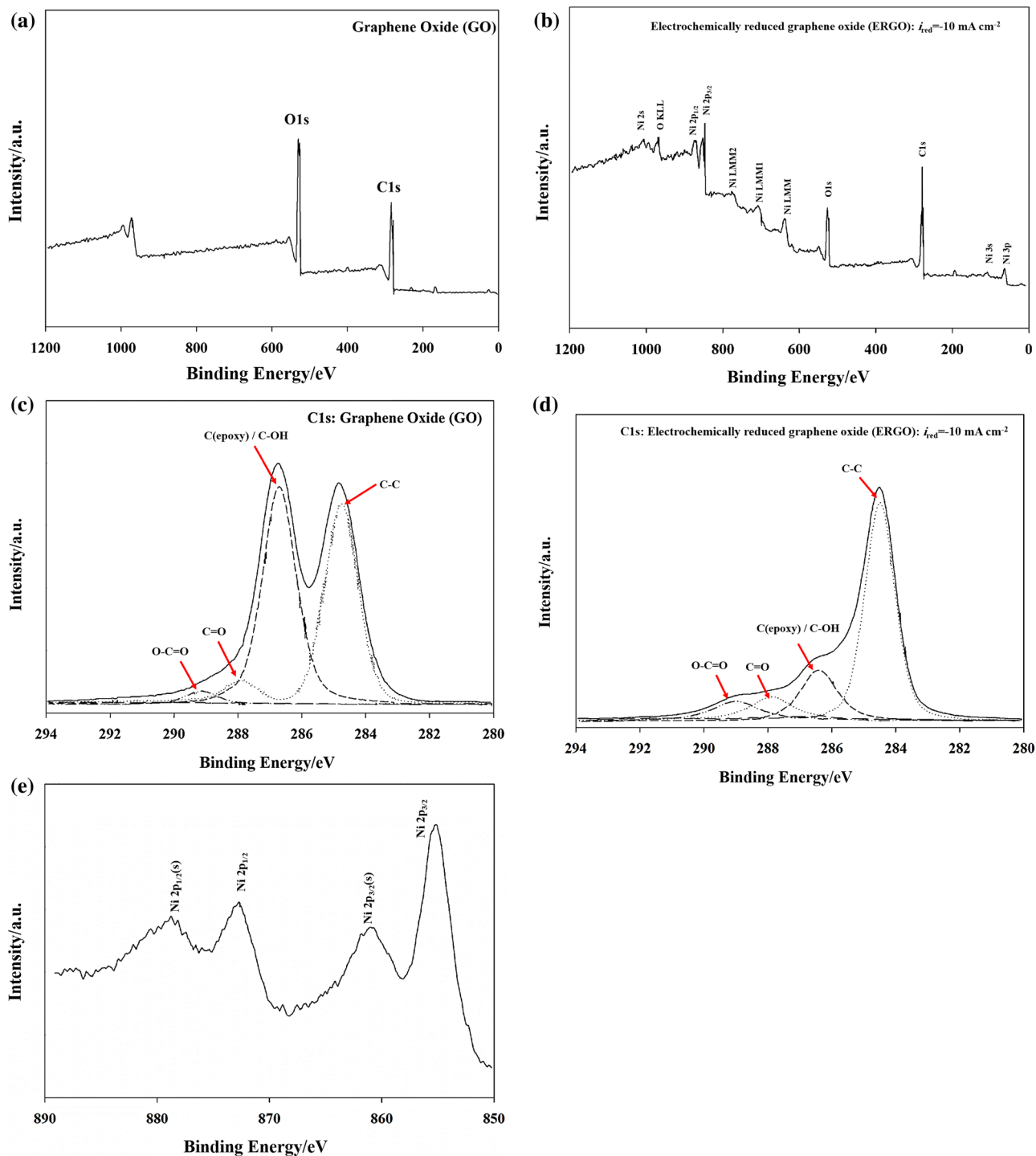


Fig. 4 a, b The XPS survey spectra of GO and ERGOs, c, d XPS C1s spectra of GO and ERGO, and e Ni 2p

($i = -5.0 \text{ mA cm}^{-2}$), 0.65Ω ($i = -20.0 \text{ mA cm}^{-2}$), and 2.7Ω (Ni–NiO foam). The radius of semicircle for all of ERGO/Ni–NiO foam electrodes were smaller than that of Ni–NiO foam, which suggested a lower charge transfer resistance for ERGO/Ni–NiO foam due to the introduction of graphene

closely related to diffusion resistance of electrolyte in electrode pores and the proton diffusion in the host material, which is a good indication of capacitive nature for porous electrodes. The almost vertical shape of this straight line indicates the swift diffusion of ions from the bulk of the electrolyte and the adsorption onto the electrode surface.

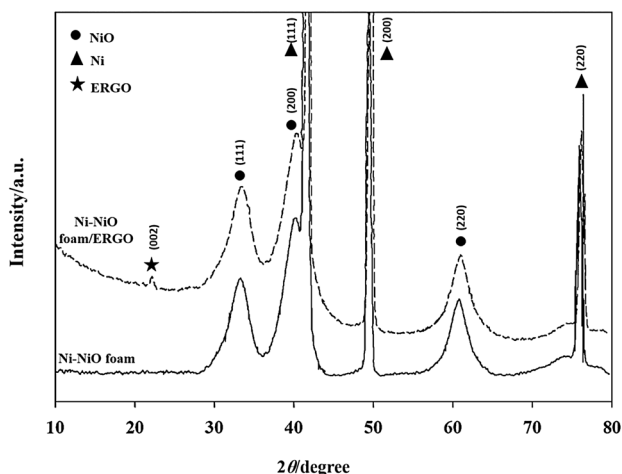


Fig. 5 The X-ray diffraction patterns of the Ni–NiO foam/ERGO film and Ni–NiO foam

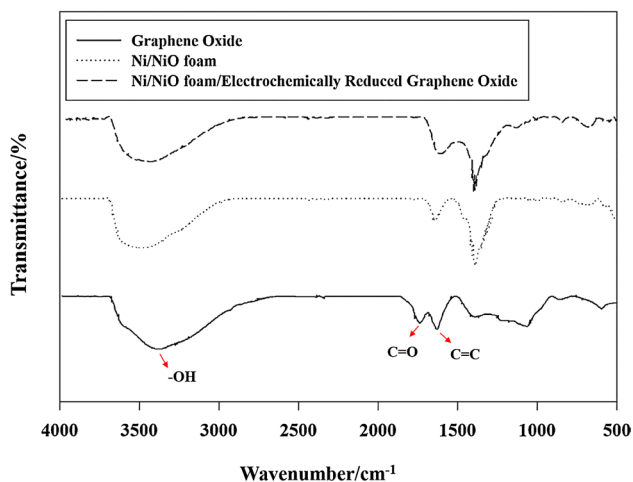


Fig. 6 The FT-IR spectra of GO, Ni–NiO foam, and Ni–NiO foam/ERGO

The Z_w values obtained for ERGO/Ni–NiO foam composite electrodes are as follows: $0.652 \Omega s^{-0.5}$ ($i = -1.8 \text{ mA cm}^{-2}$), $0.601 \Omega s^{-0.5}$ ($i = -3.0 \text{ mA cm}^{-2}$), $0.532 \Omega s^{-0.5}$ ($i = -5.0 \text{ mA cm}^{-2}$), $0.478 \Omega s^{-0.5}$ ($i = -5.0 \text{ mA cm}^{-2}$), $0.512 \Omega s^{-0.5}$ ($i = -20.0 \text{ mA cm}^{-2}$), and $0.7477 \Omega s^{-0.5}$ (Ni–NiO foam). Moreover, the ascending trend of straight line slope by increasing current density at -10 mA cm^{-2} revealed a decrease in the Warburg resistance. The desirable contact resistance between the ERGO film and foam and low resistance composite resulted in a high charge–discharge rate of the Ni–NiO foam/ERGO in the supercapacitor performance [20].

According to the CV curves (Fig. 9a), the typical reduction–oxidation pair of NiO at -0.1 to 0.5 V in the 1 M KOH solution was found by the following reaction [39]:

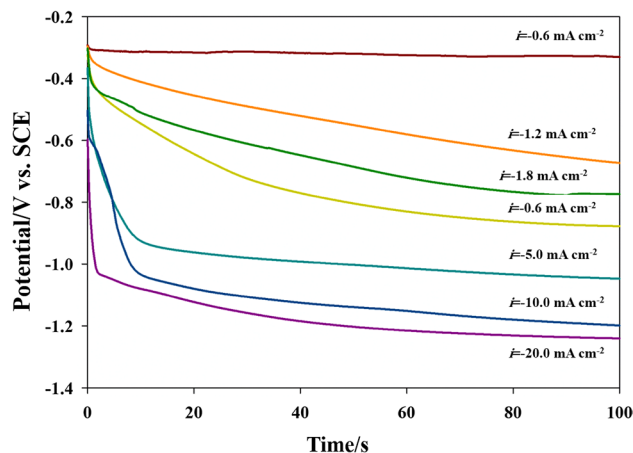


Fig. 7 Corresponding CPs to the electrochemical reduction of Ni–NiO foam/ERGO in 1 M KOH

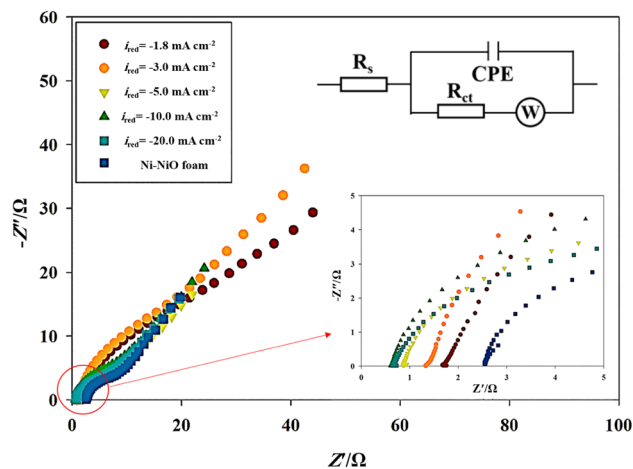
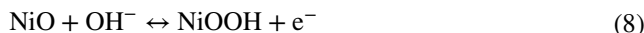


Fig. 8 The Nyquist plots of the Ni–NiO foam/ERGO electrode fabricated under the various reduction constant currents



The CV curves of the Ni–NiO foam electrode in a 1 M KOH aqueous electrolyte at various scan rates ranging from 1 to 100 mV s^{-1} are illustrated in Fig. 9a. According to the redox mechanism, almost all of the CV curves represent the behavior of a pseudocapacitive capacitance [40]. The anodic peak (positive current density) corresponds to the oxidation of NiO to NiOOH, while the cathodic peak (negative current density) is attributed to the reverse reduction process. Inset of Fig. 9a shows the CV curves of the ERGO at scan rates of 10 , 20 , 50 , and 100 mV s^{-1} . The graphene sheets demonstrate a quasi-rectangular shape expected for an ideal capacitor representing a near electrical double-layer capacitive behavior. With an increase in the scan rate, the current response increased accordingly,

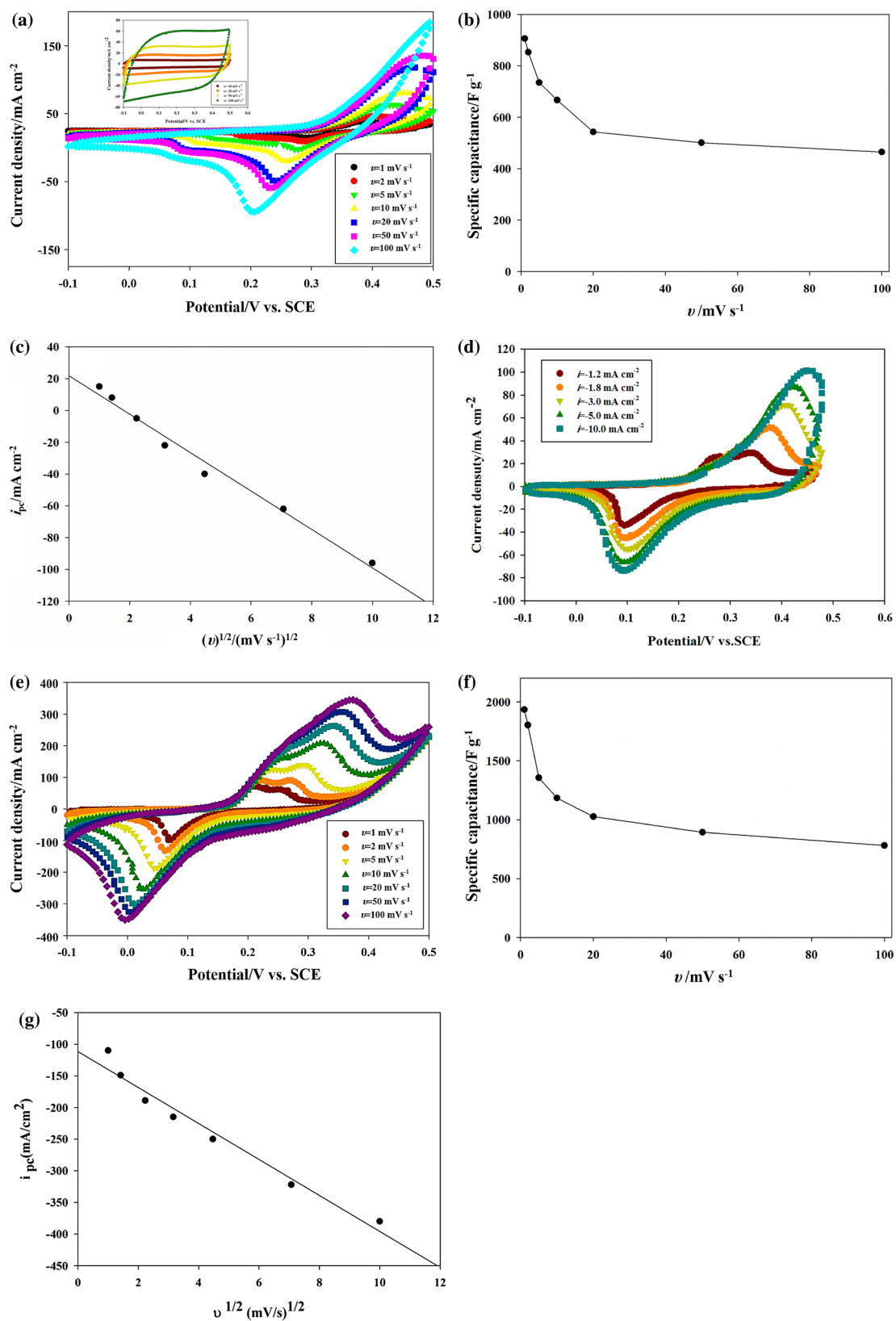


Fig. 9 The CV curves, average specific capacitance, and cathodic peak current versus the square root of the scan rate for **a–c** the Ni–NiO foam, **d** CV of Ni–NiO/ERGO prepared at various reduction current density electrodes at a scan rate of 1 mV s^{-1} and **e–g** The CV

curves, average specific capacitance, and cathodic peak current versus the square root of the scan rate for Ni–NiO foam/ERGO reduced at -10 mA cm^{-2}

and the CV profiles remained quasi-rectangular at a high scan rate of 100 mV s^{-1} , signifying low ESR, and fast diffusion of electrolyte ions through the ERGO electrodes. The specific capacitance values for the Ni–NiO foam (Fig. 9b) electrode at scan rates of 1, 2, 5, 10, 20, 50, and 100 mV s^{-1} were 906, 853, 735, 667, 543, 501 and 465 F g^{-1} , respectively.

Figure 9d shows the CV curves of Ni–NiO foam/ERGO obtained at various reduction densities with a scan rate of 1 mV s^{-1} . Apparently, the current output in the CV curves throughout the scan range for the reduction density of -10 mA cm^{-2} is obviously higher than that of reduction density at the same scan rate, indicating the higher specific capacitance. The Ni–NiO/ERGO hybrid reduced at -10 mA cm^{-2} exhibited specific capacitances of 1935, 1803, 1357, 1184, 1027, 903, and 781 F g^{-1} at 1, 2, 5, 10, 20, 50, and 100 mV s^{-1} , respectively (Fig. 9e, f). The current densities of the redox couple peaks for the Ni–NiO foam/ERGO composite are higher than those of the Ni–NiO foam and ERGO film. This indicates that the Ni–NiO foam/ERGO hybrid film has a much higher electrochemical activity than the Ni–NiO foam and ERGO, mainly due to this fact that the presence of the underlying ERGO film provides more active sites for the redox reaction. Furthermore, the negative shift of the onset potential of the oxidation reaction indicated a decrease in an energy barrier required for the NiO/NiOOH reaction, denoting the improvement of the reaction kinetics and electrochemical activities of the NiO in the presence of a graphene layer. As shown in Fig. 9c, g, an increase of the scan rate causes to obtain a more negative cathodic peak. Since there was a linear dependency between the peak currents, i_{pc} (cathodic peak current), and square root of scan rates from 1 to 100 mV s^{-1} , it was deduced that the redox reaction of the Ni–NiO and Ni–NiO/ERGO electrodes in KOH electrolyte were controlled by diffusion process on the electrode surface.

The Pseudocapacitance behavior of the Ni–NiO foam is shown in galvanostatic discharge curves of Fig. 10a. The slope variation from 0.5 to 0.33 V is due to the redox reaction between Ni–NiO foam/ERGO and the electrolyte interface and electrochemical adsorption–desorption [41]. A rapid voltage drop was found at voltages below 0.33 V, which reveals the common double-layer-capacitance behavior because of simple charge separation between the electrode and electrolyte. Figure 10c shows the GCD curves of Ni–NiO foam/ERGO obtained at various reduction densities with a discharge current of 1 A g^{-1} . The discharge time under the GCD curves for Ni–NiO foam composite at reduction density of -10 mA cm^{-2} is much longer than that of reduction density at the same current density, confirming the higher specific capacitance.

According to the discharge–time data, the specific capacitances of the hybrid electrode are calculated and

plotted in Fig. 10d, e. Inset of Fig. 10d shows the GCD curves of the three samples in the voltage range of 0–0.5 V (vs. SCE) at a constant current density of 1.0 A/g . The graphene electrode presents a nearly linear discharge curve, characteristic for the capacitive behavior of a typical double layer, with a specific capacitance of 286 F/g . In Ni–NiO foam/ERGO, the linear part could be attributed to pure double-layer capacitance behavior from the charge separation at the electrode/electrolyte interface. Since faradaic redox reaction is usually accompanied by the double-layer charge–discharge process, the non-linear part could be correlated to a combination behavior of double-layer capacitance and pseudocapacitance.

The Ni–NiO/ERGO hybrid reduced at -10 mA cm^{-2} displayed specific capacitances of 1995, 1836, 1199, 932, and 806 F g^{-1} at 1, 2, 5, 10, and 20 A g^{-1} , respectively (Fig. 10e), which were much higher than those attained from the Ni–NiO foam [924, 841, 694, 501, and 462 F g^{-1} , respectively (Fig. 10b)]. This significant increase of specific capacitance can correspond to the special structure of the composite films. High surface area for redox reactions is due to the vertically aligned nano dendrites, porous structure, and numerous electroactive sites of the Ni–NiO foam/ERGO. Therefore, such a special architecture of ERGO and the double NiO layers are so promising for supercapacitor application. The electrochemical stability electrode was assessed by a degradation test performed with 6000 GCD cycles at a high charge/discharge current density of 20 A g^{-1} (Fig. 10f). During the first 400 cycles, specific capacitance was increased. This phenomenon can be described by the activation of electrode leading to the increase in the number of available active sites and facilitating the diffusion of trapped ions. The Ni–NiO foam and Ni–NiO foam/ERGO composite electrodes exhibited 18.4 and 4.9% capacity decay after 6000 cycles of charging and discharging at a 20 A g^{-1} current density, respectively. The unique morphology and stable structure of the Ni–NiO foam/ERGO composite is the main reason for such excellent cycling stability. Therefore, the Ni–NiO foam/ERGO composite electrode can be an appropriate candidate for pseudocapacitors due to its high electrochemical stability.

This superior performance could be described by the high specific surface area of ERGO, easing the collection and transportation of electrons during the cycling process. The nanocomposite fabricated in this study exhibited much higher capacity retention at high current densities than previous reported materials such as Ni/NiO/RGO, nickel-based compound-graphene sheet, NiO/rGO, NiO, and graphene skeletons supported by nickel molybdate nanowire (Table 1).

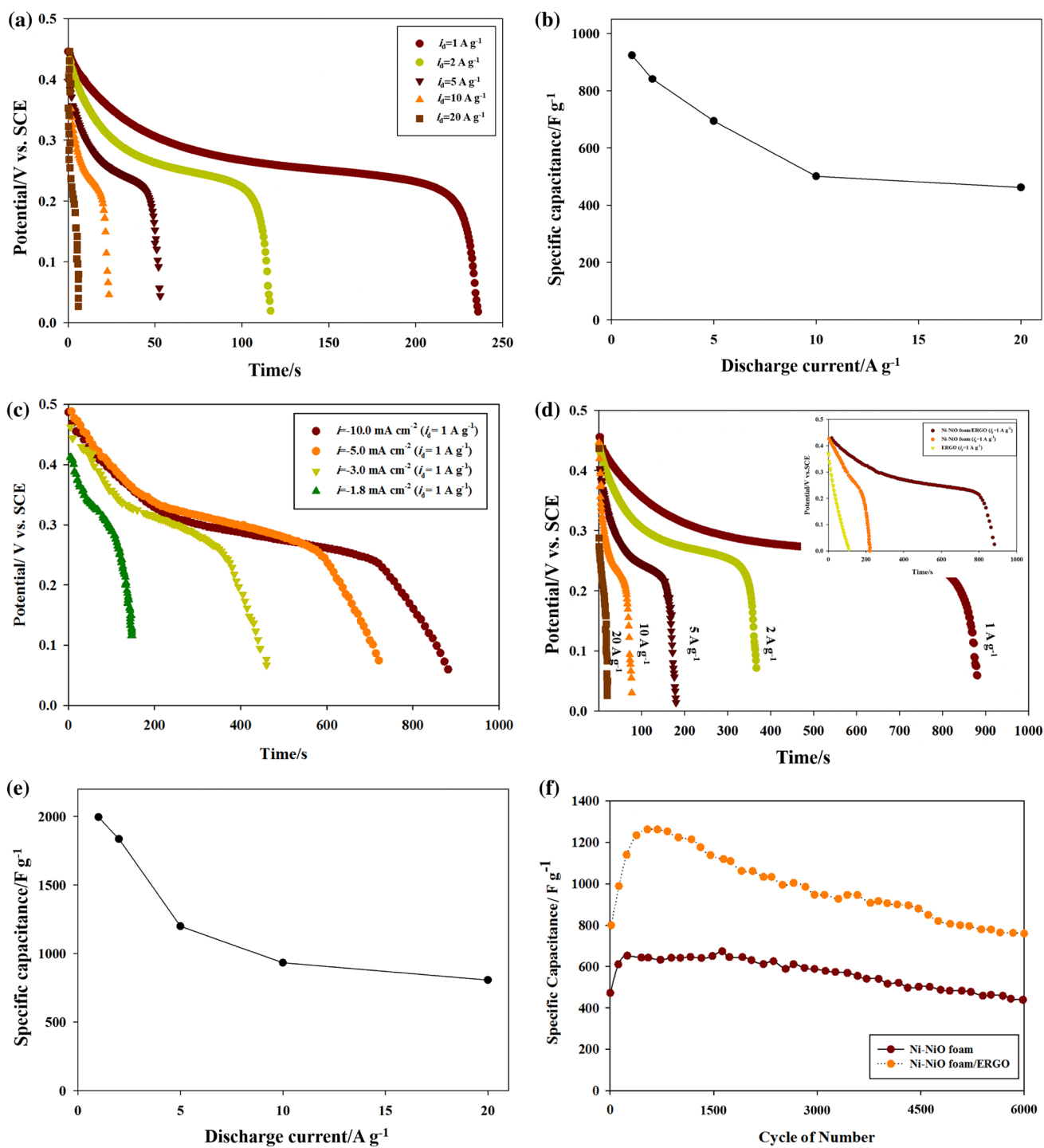


Fig. 10 The GCD and average specific capacitance at the various discharge current densities for **a**, **b** the Ni–NiO foam, **c** GCD curves of Ni–NiO foam/ERGO prepared at various reduction current density electrodes at a current density of 1 A g^{-1} , **d**, **e** The GCD and average

specific capacitance at the various discharge current densities for Ni–NiO foam/ERGO reduced at -10 mA cm^{-2} , and **f** the cyclic stability of electrodes at a current density of 20 A g^{-1}

4 Conclusion

In this research, a simple galvanic displacement reaction was employed to fabricate dendritic Cu-dealloyed nanoporous

Ni–NiO foam. Furthermore, a novel hybrid method incorporating drop casting and galvanostatic process was deployed to produce graphene-developed hybrid on the Ni–NiO foam. The interaction between the Ni–NiO complexes and

Table 1 The comparison of the specific capacities of Ni–NiO foam/ERGO fabricated in this study and the literature

Electrode material	Specific capacitance (F g ⁻¹)	Capacitance retention (%)	Reference
Ni/NiO/RGO	1027 at 2 A g ⁻¹	92.95% retention after over 1000 cycles	[42]
Nickel-based compound-graphene sheet	1864 at 1 A g ⁻¹	78% retention after over 5000 cycles	[43]
NiO/rGO	770 at 1 A g ⁻¹	–	[44]
NiO	810 at 1 A g ⁻¹	89% retention after over 1000 cycles	[44]
Graphene skeletons supported nickel molybdate nanowire	1194 at 12 mA cm ⁻²	87.3% retention after 2000 cycles	[45]
Ni–NiO Foam/ERGO	1995 at 1 A g ⁻¹	95.1% retention after 6000 cycles	This work

graphene resulted in an effective electrode–electrolyte interfacial area, the fast direction for the transport of electrolyte ions, and an easy Faraday reaction. The manufactured composite electrode demonstrated a specific capacitance of up to 1995 F g⁻¹ at a current density of 1 A g⁻¹ in a 1 M KOH solution. In addition, the electrode presented impressive cycling stability with capacity retention of 95.1% after 6000 cycles. It was concluded that the Ni–NiO/ERGO hybrid electrode materials have a promising application in electrochemical energy storages due to their superior electrochemical performance, cost effectiveness, and easy fabrication.

References

- Zhao X, Sánchez BM, Dobson PJ, Grant PS (2011) The role of nanomaterials in redox-based supercapacitors for next generation energy storage devices. *Nanoscale* 3(3):839–855
- Simon P, Gogotsi Y (2008) Materials for electrochemical capacitors. *Nat Mater* 7(11):845
- Nikolić ND, Popov KI, Pavlović LJ, Pavlović MG (2006) The effect of hydrogen codeposition on the morphology of copper electrodeposits. I. The concept of effective overpotential. *J Electro Chem* 588(1):88–98
- Nikolić ND, Branković G, Pavlović MG, Popov KI (2008) The effect of hydrogen co-deposition on the morphology of copper electrodeposits. II. Correlation between the properties of electrolytic solutions and the quantity of evolved hydrogen. *J Electro Chem* 621(1):13–21
- Cherevko S, Kulyk N, Chung CH (2012) Nanoporous Pt@Au_xCu_{100-x} by hydrogen evolution assisted electrodeposition of Au_xCu_{100-x} and galvanic replacement of Cu with Pt: electrocatalytic properties. *Langmuir* 28(6):3306–3315
- Cherevko S, Kulyk N, Chung CH (2012) Nanoporous palladium with sub-10 nm dendrites by electrodeposition for ethanol and ethylene glycol oxidation. *Nanoscale* 4(1):103–105
- Cherevko S, Kulyk N, Chung CH (2012) Pulse-reverse electrodeposition for mesoporous metal films: combination of hydrogen evolution assisted deposition and electrochemical dealloying. *Nanoscale* 4(2):568–575
- Jiang J, Li Y, Liu J, Huang X, Yuan C, Lou XWD (2012) Recent advances in metal oxide-based electrode architecture design for electrochemical energy storage. *Adv Mater* 24(38):5166–5180
- Srivastava M, Singh J, Kuila T, Layek RK, Kim NH, Lee JH (2015) Recent advances in graphene and its metal-oxide hybrid nanostructures for lithium-ion batteries. *Nanoscale* 7(11):4820–4868
- Wang F, Kozawa D, Miyauchi Y, Hiraoka K, Mouri S, Ohno Y, Matsuda K (2015) Considerably improved photovoltaic performance of carbon nanotube-based solar cells using metal oxide layers. *Nat Commun* 6:6305
- Tao K, Li P, Kang L, Li X, Zhou Q, Dong L, Liang W (2015) Facile and low-cost combustion-synthesized amorphous mesoporous NiO/carbon as high mass-loading pseudocapacitor materials. *J Power Sources* 293:23–32
- Xu YT, Guo Y, Li C, Zhou XY, Tucker MC, Fu XZ, Wong CP (2015) Graphene oxide nano-sheets wrapped Cu₂O microspheres as improved performance anode materials for lithium ion batteries. *Nano Energy* 11:38–47
- Bonaccorso F, Colombo L, Yu G, Stoller M, Tozzini V, Ferrari AC, Pellegrini V (2015) Graphene, related two-dimensional crystals, and hybrid systems for energy conversion and storage. *Science* 347:1246501
- Wei W, Yang S, Zhou H, Lieberwirth I, Feng X, Müllen K (2013) 3D graphene foams cross-linked with pre-encapsulated Fe₃O₄ nanospheres for enhanced lithium storage. *Adv Mater* 25(21):2909–2914
- Cao X, Yin Z, Zhang H (2014) Three-dimensional graphene materials: preparation, structures and application in supercapacitors. *Energ Environ Sci* 7(6):1850–1865
- Feng L, Zhu Y, Ding H, Ni C (2014) Recent progress in nickel based materials for high performance pseudocapacitor electrodes. *J Power Sources* 267:430–444
- Yuan C, Wu HB, Xie Y, Lou XWD (2014) Mixed transition-metal oxides: design, synthesis, and energy-related applications. *Angew Chem Int Edit* 53(6):1488–1504
- Xia XH, Tu JP, Zhang YQ, Mai YJ, Wang XL, Gu CD, Zhao XB (2011) Three-dimensional porous nano-Ni/C₆(OH)₂ nanoflake composite film: a pseudocapacitive material with superior performance. *J Phys Chem C* 115(45):22662–22668
- Zhuo K, Jeong M, Chung CH (2013) Dendritic nanoporous nickel oxides for a supercapacitor prepared by a galvanic displacement reaction with chlorine ions as an accelerator. *RSC Adv* 3(31):12611–12615
- Yuan C, Li J, Hou L, Zhang X, Shen L, Lou XWD (2012) Ultrathin mesoporous NiCo₂O₄ nanosheets supported on Ni foam as advanced electrodes for supercapacitors. *Adv Funct Mater* 22(21):4592–4597
- Kundu M, Liu L (2013) Direct growth of mesoporous MnO₂ nanosheet arrays on nickel foam current collectors for high-performance pseudocapacitors. *J Power Sources* 243:676–681
- Yang D, Velamakanni A, Bozoklu G, Park S, Stoller M, Piner RD, Ruoff RS (2009) Chemical analysis of graphene oxide films after heat and chemical treatments by X-ray photoelectron and micro-Raman spectroscopy. *Carbon* 47(1):145–152

23. Ferrari AC, Meyer JC, Scardaci V, Casiraghi C, Lazzeri M, Mauri F, Geim AK (2006) Raman spectrum of graphene and graphene layers. *Phys Rev Lett* 97(18):187401
24. Ramesha GK, Sampath S (2009) Electrochemical reduction of oriented graphene oxide films: an in situ Raman spectroelectrochemical study. *J Phys Chem C* 113(19):7985–7989
25. Yan J, Sun W, Wei T, Zhang Q, Fan Z, Wei F (2012) Fabrication and electrochemical performances of hierarchical porous Ni(OH)₂ nanoflakes anchored on graphene sheets. *J Mater Chem* 22(23):11494–11502
26. Zu SZ, Han BH (2009) Aqueous dispersion of graphene sheets stabilized by pluronic copolymers: formation of supramolecular hydrogel. *J Phys Chem C* 113(31):13651–13657
27. Zhou W, Cao X, Zeng Z, Shi W, Zhu Y, Yan Q, Zhang H (2013) One-step synthesis of Ni₃S₂ nanorod@Ni(OH)₂ nanosheet core-shell nanostructures on a three-dimensional graphene network for high-performance supercapacitors. *Energ Environ Sci* 6(7):2216–2221
28. Jiang C, Zhan B, Li C, Huang W, Dong X (2014) Synthesis of three-dimensional self-standing graphene/Ni(OH)₂ composites for high-performance supercapacitors. *RSC Adv* 4(35):18080–18085
29. Zhou G, Wang DW, Yin LC, Li N, Li F, Cheng HM (2012) Oxygen bridges between NiO nanosheets and graphene for improvement of lithium storage. *ACS Nano* 6(4):3214–3223
30. Kitaura R, Imazu N, Kobayashi K, Shinohara H (2008) Fabrication of metal nanowires in carbon nanotubes via versatile nanotemplate reaction. *Nano Lett* 8(2):693–699
31. Zhou J, Song H, Ma L, Chen X (2011) Magnetite/graphene nanosheet composites: interfacial interaction and its impact on the durable high-rate performance in lithium-ion batteries. *Rsc Adv* 1(5):782–791
32. Peng XY, Liu XX, Diamond D, Lau KT (2011) Synthesis of electrochemically-reduced graphene oxide film with controllable size and thickness and its use in supercapacitor. *Carbon* 49(11):3488–3496
33. Park S, Ruoff RS (2009) Chemical methods for the production of graphenes. *Nat Nanotechnol* 4(4):217
34. Hilder M, Winther-Jensen B, Li D, Forsyth M, MacFarlane DR (2011) Direct electro-deposition of graphene from aqueous suspensions. *Phys Chem Chem Phys* 13(20):9187–9193
35. Li W, Liu J, Yan C (2013) Reduced graphene oxide with tunable C/O ratio and its activity towards vanadium redox pairs for an all vanadium redox flow battery. *Carbon* 55:313–320
36. Marcano DC, Kosynkin DV, Berlin JM, Sinitskii A, Sun Z, Slesarev A, Tour JM (2010) Improved synthesis of graphene oxide. *ACS Nano* 4(8):4806–4814
37. Chen XA, Chen X, Zhang F, Yang Z, Huang S (2013) One-pot hydrothermal synthesis of reduced graphene oxide/carbon nanotube/ α -Ni(OH)₂ composites for high performance electrochemical supercapacitor. *J Power Sources* 243:555–561
38. Zhai T, Wang F, Yu M, Xie S, Liang C, Li C, Tong Y (2013) 3D MnO₂-graphene composites with large areal capacitance for high-performance asymmetric supercapacitors. *Nanoscale* 5(15):6790–6796
39. Min S, Zhao C, Chen G, Qian X (2014) One-pot hydrothermal synthesis of reduced graphene oxide/Ni(OH)₂ films on nickel foam for high performance supercapacitors. *Electrochim Acta* 115:155–164
40. Wang H, Casalongue HS, Liang Y, Dai H (2010) Ni(OH)₂ nanoplates grown on graphene as advanced electrochemical pseudocapacitor materials. *J Am Chem Soc* 132(21):7472–7477
41. Sugimoto W, Iwata H, Yasunaga Y, Murakami Y, Takasu Y (2003) Preparation of ruthenic acid nanosheets and utilization of its interlayer surface for electrochemical energy storage. *Angew Chem Int Edit* 42(34):4092–4096
42. Zhu Y, Chu W, Wang N, Lin T, Yang W, Wen J, Zhao XS (2015) Self-assembled Ni/NiO/RGO heterostructures for high-performance supercapacitors. *RSC Adv* 5(95):77958–77964
43. Zhang LB, Yang SR, Wang JQ, Xu Y, Kong XZ (2015) A facile preparation and electrochemical properties of nickel based compound-graphene sheet composites for supercapacitors. *Chinese Chem Lett* 26(5):522–528
44. Zhu X, Dai H, Hu J, Ding L, Jiang L (2012) Reduced graphene oxide-nickel oxide composite as high performance electrode materials for supercapacitors. *J Power Sources* 203:243–249
45. Liu X, Zhang K, Yang B, Song W, Liu Q, Jia F, Li J (2016) Three-dimensional graphene skeletons supported nickel molybdate nanowire composite as novel ultralight electrode for supercapacitors. *Mater Lett* 164:401–404

Affiliations

Majid Mirzaee¹ · Changiz Dehghanian¹ · Sahand Sarbishei²

✉ Changiz Dehghanian
cdehghan@ut.ac.ir

Majid Mirzaee
majidmirzaee7@gmail.com

¹ College of Engineering, School of Metallurgy and Materials Engineering, University of Tehran, P.O. Box 11155-4563, Tehran, Iran

² Department of Materials Engineering, The University of British Columbia, Vancouver, BC V6T 1Z4, Canada